Advanced Functional Materials

ADVANCED FUNCTIONAL MATERIALS
www.afm-journal.de

RESEARCH ARTICLE OPEN ACCESS

Self-Assembled Lipids as Soft Dielectrics

Hao Yang[1,2] | Yiding Li[3] | Jitong Ren[2,4] | Yu Shi[5] | Charles M. Schroeder[3,6]

[1]Department of Materials Science and Engineering, University of Illinois Urbana-Champaign, Urbana, Illinois, USA | [2]Beckman Institute For Advanced Science and Technology, University of Illinois Urbana-Champaign, Urbana, Illinois, USA | [3]Department of Chemical and Biological Engineering, Princeton University, Princeton, New Jersey, USA | [4]Department of Chemical and Biomolecular Engineering, University of Illinois Urbana-Champaign, Urbana, Illinois, USA | [5]Department of Chemistry, University of Illinois Urbana-Champaign, Urbana, Illinois, USA | [6]Princeton Materials Institute, Princeton University, Princeton, New Jersey, USA

Correspondence: Charles M. Schroeder (cschroeder@princeton.edu)

Received: 31 March 2026 | **Revised:** 26 June 2026 | **Accepted:** 30 July 2026

Keywords: bioelectronics | dielectrics | EGaIn | lipid bilayers | molecular electronics

ABSTRACT

Lipid membranes are ubiquitous structures in nature that enable efficient charge separation and electrochemical gradients across interfaces. Despite recent progress in understanding the structural properties of lipid membranes, the electronic properties of lipid assemblies in the solid state are not fully understood. Here, we show that dehydrated lipid assemblies serve as soft dielectric materials for molecular electronics. Polymer-supported lipid bilayers are prepared on gold electrodes via vesicle fusion, yielding uniform films with sub-nanometer roughness determined by atomic force microscopy (AFM). The dielectric properties of dehydrated lipid assemblies are characterized using the soft-contact liquid-metal eutectic gallium-indium (EGaIn) technique. Capacitance measurements in a parallel-plate geometry enable determination of the dielectric constant of lipid bilayers, which is systematically tuned via molecular structure, composition, and assembly conditions. Lipid assemblies formed with increased cholesterol content or at lower temperatures exhibit reduced surface roughness, consistent with enhanced molecular ordering upon dehydration. These results highlight the role of self-assembly on the structural and electronic properties of dehydrated lipids and establish new avenues for biologically inspired soft dielectrics.

1 | Introduction

Lipids are key components of biological membranes and play a central role in wide range of biochemical processes. In nature, lipid membranes serve as both a structural scaffold and a dynamic functional platform for membrane proteins [1, 2]. Lipid bilayers exhibit intriguing electronic properties such as high resistivity and capacitance, thereby serving as natural charge separation motifs in biology [3, 4]. Biological membranes store and transmit electrical signals due to their intrinsic electrochemical properties, as observed in the propagation of action potentials in neuron cells [5, 6]. Moreover, amphiphilic lipid molecules spontaneously self-assemble into nanometer-thick bilayers and micron-scale structures such as vesicles, which are readily visualized under an optical microscope [7]. The fluid nature of lipid bilayers further allows for rapid repair of structural disruptions, giving rise to self-healing behavior [8].

Lipid-based materials offer several advantages for applications in microelectronics owing to their intrinsic electronic properties, spontaneous self-assembly behavior, and potential for large-area uniformity. Top-down fabrication of nanometer-thick dielectric layers for dynamic random access memory (DRAM) capacitors is challenging [9, 10], where it is desirable to achieve nanometer

Hao Yang and Yiding Li contributed equally to this work.

-scale dielectric layers with minimum roughness and uniform thickness over high-aspect-ratio structures [11]. Traditional fabrication methods such as atomic layer deposition and atomic layer etching typically require energy-intensive processes and harsh chemical environments [12, 13]. In contrast, self-assembled lipids offer a potential alternative strategy using a bio-inspired material that naturally forms ultrathin dielectric layers with reduced demands on fabrication [14].

The electronic properties of lipid bilayers have been extensively studied in solvated electrochemical environments [3, 14, 15], but the vast majority of electronic devices operate in the solid state. Direct characterization of dehydrated lipid assemblies is therefore essential for advancing lipid-based materials for electronic applications [16]. A central challenge in using lipid bilayers as functional thin films lies in their structural fragility: bilayers tend to reorganize during dehydration, which complicates the preparation of ordered structures on solid substrates or at air-water interfaces [17, 18]. In addition, establishing reliable electrical contacts without perturbing soft materials or interfaces remains challenging, as conventional solid metallic electrodes often exert mechanical stresses that can compromise film integrity [19]. Early studies of fatty acid salt monolayers established the feasibility of using molecularly thin lipid-like assemblies as tunneling barriers [20]. However, the structure-property relationships of dehydrated phospholipid assemblies are not yet fully understood. In particular, how lipid molecular structure, assembly pathways, and dehydration-induced morphology collectively influence dielectric behavior remains an open question.

In this work, we explore the use of dehydrated lipid assemblies as soft dielectric materials. Polymer-supported lipid bilayers are formed on template-stripped gold substrates, which serve as a bottom electrode, and a liquid metal (eutectic gallium–indium alloy, EGaIn) is used as the top electrode. EGaIn provides a soft, non-invasive contact ideal for characterizing the electronic properties of soft matter systems [21]. Surface characterization techniques including contact angle measurements, atomic force microscopy (AFM), and infrared spectroscopy are further used to study lipid assembly and evaluate film morphology and uniformity. Following fabrication and structural characterization, the capacitance and breakdown voltage of lipid assemblies are measured using a parallel-plate capacitor geometry (Figure 1). Our results demonstrate that the structure and dielectric properties of lipid assemblies can be systematically tuned through molecular design (lipid tail length), composition (cholesterol content), and assembly conditions (temperature), with dehydration playing a central role in establishing the resulting structure–property relationships. Overall, these finding suggest that self-assembled lipids form insulating, large-area films with controllable dielectric behavior.

2 | Results and Discussion

2.1 | Vesicle Preparation

We began by fabricating self-assembled polymer-supported lipid bilayers on gold substrates. Template-stripped gold surfaces with extremely low surface roughness were prepared as described in prior work [22]. Several lipids with varying acyl-chain lengths were used in this study: 1,2-dimyristoyl-sn-glycero-3-phosphocholine (C14), 1,2-dioleoyl-sn-glycero-3-phosphocholine (DOPC, C18), and 1,2-dierucoyl-sn-glycero-3-phosphocholine (C22). Lipids were purchased from Avanti Polar Lipids and used as received (**Materials and Methods**). Phosphatidylcholine (PC) lipids were selected because they are widely used as model membrane-forming lipids, commercially accessible, and readily form vesicles for supported lipid assembly. PC lipids have phase-transition temperatures below the assembly conditions used here, such that vesicles remain in a fluid phase during deposition. Membrane fluidity promotes vesicle adhesion, rupture, fusion, and reorganization on PDL-functionalized gold surfaces, enabling formation of supported lipid assemblies prior to dehydration.

We first attempted to directly assemble lipid C18 onto template-stripped gold surfaces, but the structure of lipid assemblies on bare gold surfaces was significantly disrupted upon drying, consistent with prior work showing that dehydration disrupts the bilayer architecture due to surface tension-induced stresses [23, 24]. To overcome this issue, polymer-supported lipid bilayers were formed on template-stripped gold surfaces using poly-D-lysine (PDL), which is commonly used to enhance surface adhesion in biological systems [25]. Contact angle measurements revealed that template-stripped gold surfaces are hydrophobic, but the PDL-coated gold surfaces were generally hydrophilic (Figure S1). PDL-functionalized gold surfaces were incubated in a solution containing C18 lipid, followed by gentle rinsing with deionized water and drying under vacuum. Self-assembled lipids on gold surfaces were characterized using attenuated total reflectance-Fourier-transform infrared (ATR-FTIR) spectroscopy (Figure S2), with spectral features consistent with the presence of lipid molecules.

We next prepared ordered lipid assemblies over large, micron-scale areas for electronic measurements. To achieve large-area uniformity, lipid molecules were assembled on gold substrates using a vesicle-fusion process, wherein vesicles adsorb, rupture, and spread upon contact with PDL-functionalized gold surfaces, reorganizing into a continuous bilayer (Supplementary Information, Section 3) [26, 27]. Two approaches were used to prepare lipid vesicles. In the first method, C18 lipids were dispersed in water and sonicated, yielding a complex mixture of spontaneously assembled small unilamellar vesicles and multilamellar aggregates with characteristic diameters ranging from approximately 100 to 500 nm [28]. In the second method, giant unilamellar vesicles (GUVs) were generated using an electroformation method, yielding micrometer-sized vesicles, followed by adsorption and spreading onto solid substrates (Figures S3 and S4) [29]. Lipid films formed by these two different vesicle adsorption methods exhibited strikingly different morphologies (Figure 2). AFM topography images show that the sonicated lipid samples produced rough and uneven surfaces (Figure 2a), with AFM phase images showing patchy contrast indicative of heterogeneous surface morphologies with variable tip–sample interactions and (Figure 2b). In contrast, GUV-derived films show decreased roughness (Figure 2c) with a uniform phase behavior over micron-scale areas (Figure 2d), consistent with a continuous and homogeneous lipid layer. Electroformation favors the formation of unilamellar vesicles, which provide

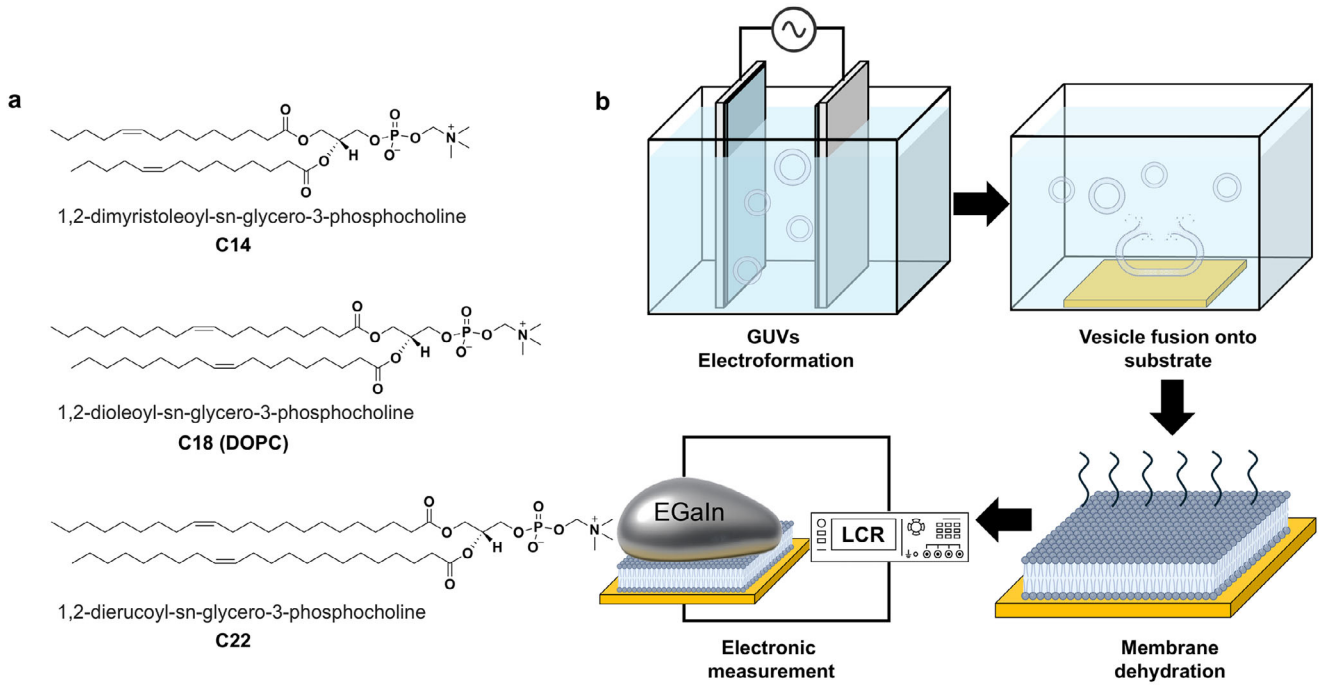

FIGURE 1 | Chemical structure of lipid molecules and overview of lipid sample preparation and electronic measurements. (a) Chemical structures of lipids with varying hydrophobic tail lengths. (b) Overview and schematic of lipid bilayer fabrication process and electronic measurements.

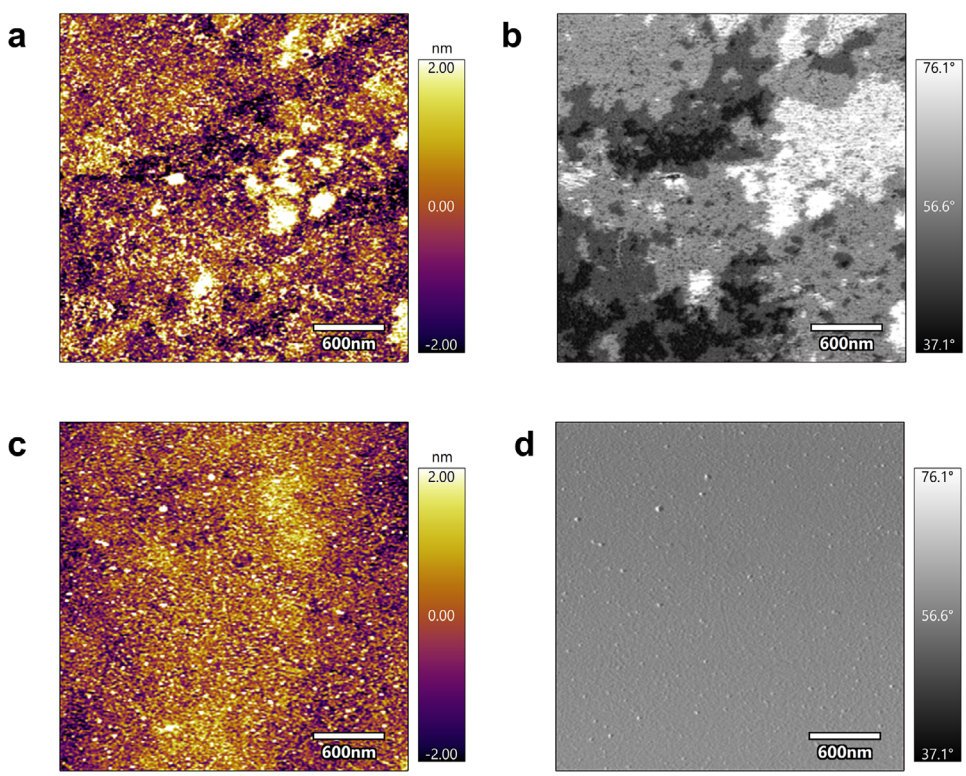

FIGURE 2 | Surface characterization of dehydrated lipid layers. (a) AFM characterization of lipid assembled layers formed by sonicating C18 lipid in water for 10 min with (b) the corresponding phase contrast image. (c) AFM topography image of a C18 lipid layer formed by adsorption and spreading of giant unilamellar vesicles (GUVs) with (d) corresponding phase contrast image.

continuous membrane material that can rupture and spread on PDL-functionalized gold surfaces, whereas sonication generates heterogeneous mixtures of small vesicles, multilamellar vesicles, and lipid aggregates that lead to patchy surface assemblies. However, supported-bilayer formation is governed by a balance between surface adhesion, membrane bending and curvature energy, hydration repulsion, lipid composition, and temperature. Well-defined extruded unilamellar vesicles often rupture on hydrophilic substrates, and smaller vesicles generally exhibit higher curvature-induced stresses; however, substrate chemistry and the onset of rupture above a critical adsorbed coverage are also decisive factors [23, 27, 30–33]. Conversely, single-GUV studies have shown that adsorbed GUVs can deform, rupture, and spread into planar bilayer patches through several pathways [34]. Results from the present studies compare a heterogeneous sonicated dispersion with an electroformed GUV preparation rather than a systematic SUV vs. GUV size series. The smoother GUV-derived films may therefore reflect combined differences in lamellarity, dispersity, membrane continuity, and substrate-specific rupture kinetics. Based on these results, GUVs were used to prepare polymer-supported lipid assemblies on gold surfaces for electronic measurements.

2.2 | Structural Characterization

Film thickness serves as a critical parameter for determining the dielectric constant of electroactive materials. We characterized lipid layer thicknesses using an AFM scratching method, wherein a controlled force of 100 nN is applied in contact mode to selectively remove the soft organic layer without damaging the gold substrate (Figure S5) [35]. The height difference between the regions with and without the organic layer is used to determine the film thickness (Figure 3). Height histograms are constructed from AFM topography scans (Figure 3b), revealing two distinct Gaussian distributions for regions with and without the organic layer, and the peak-to-peak separation is used to determine the film thickness. The C18 lipid assembled on PDL-adsorbed gold surfaces at 45°C was found to have a thickness of 5.8 nm. After correcting for the 0.9 nm thickness of the PDL linker (Figure S6), the thickness of the C18 layer (alone) was 4.9 nm, which is larger than C18 bilayer thicknesses reported in prior work (e.g., 3.9 nm by Kucerka et al. [36], 3.5 nm by Tristram-Nagle et al. [37]). The slightly larger thickness in our system is attributed in part to the elevated temperature of lipid assembly in our work (45°C), as discussed in detail below, whereas the prior structural data were obtained at room temperature (25°C). Moreover, our measurements correspond to dehydrated lipid films, and prior work has shown that the thickness of lipid bilayers increases due to lateral compression upon drying [38–42]. In particular, the area per lipid decreases during dehydration whereas the specific molecular volume remains constant, leading to a compensatory increase in height in the vertical direction. As a result, acyl chains adopt more ordered conformations and reduced mobility in the dehydrated state, resulting in slightly thicker films [38–42]. In addition, previously reported values of lipid bilayer thickness were determined from scattering techniques, whereas our results rely on AFM measurements. Nevertheless, the experimentally measured thickness values are consistent with lipid bilayer assembles, as multilayer assemblies are known to generate substantially thicker films.

We systematically varied the acyl-chain length by using different lipids denoted as C14, C18, and C22 (Figure 1). Upon increasing the lipid tail length, the film thickness increased to 5.0, 5.8, and 6.1 nm for C14, C18, and C22 respectively, when assembled at 45°C (Figures S7–S9). These results are consistent with the expected increase in molecular length for ordered assembled layers with bilayer-like structural characteristics (Figure 3d), as opposed to disordered, amorphous films. Surface roughness (*Rq*) was observed to slightly increase upon increasing the lipid tail length (Figure S10), which is attributed to the structural reorganization that occurs during dehydration, where the area per lipid (APL) decreases as the acyl chains lose flexibility and become ordered [41]. Dehydration is expected to be nonuniform due to local variations in substrate adhesion, lipid mobility, and residual water content, giving rise to nanoscale height variations. Because the amplitude of such variations is comparable to the film thickness, thicker layers are expected to show an increased apparent surface roughness.

Environmental factors such as temperature also affect the self-assembly behavior of lipid assemblies [43]. We prepared PDL-supported C18 lipid layers at 20°C, 45°C, and 60°C and characterized their morphology by AFM (Figure 3d and Figure S11–S13). At lower temperatures, the apparent film thickness was markedly reduced, whereas the apparent thickness increased at higher temperatures. These trends in lipid film thickness appear counterintuitive relative to hydrated vesicles, where increased tail disorder at elevated temperatures typically leads to lateral expansion and a slight decrease in bilayer thickness [44, 45]. Here, we attribute the increase in thickness observed at elevated temperatures to the dehydration process. Because the lipid films are dehydrated and surface-confined, the observed morphology reflects a kinetically trapped structure on a solid substrate due to dehydration-induced reorganization rather than an equilibrated hydrated bilayer. Lipid layers assembled at 60°C are initially more fluid and disordered, with larger area per lipid [46], but upon dehydration, the acyl chains coalesce and the area per lipid decreases. As the film contracts, the absence of nearby mobile lipid molecules to fill the emerging gaps results in the formation of local microvoids, consistent with results from AFM imaging (Figure S14). In this way, dehydration at elevated temperatures results in enhanced surface heterogeneities with a larger average thickness and an increase in surface roughness as determined by AFM measurements, reflecting increased structural disorder rather than a densely packed layer. On the other hand, lipid layers assembled at 20°C are initially more ordered and closely packed, which results in smaller changes in the area per lipid upon dehydration, yielding assembled films that closely resemble the original hydrated bilayer. Overall, these results suggest that the dehydration process plays a critical role in the structural properties of assembled lipid films.

We next systematically varied the cholesterol content in lipid assembles. Cholesterol intercalates between lipid acyl chains, reducing lipid tail mobility and thereby stiffening the membrane [47–49]. Cholesterol was added to C18 lipid at 0 mol%, 15 mol%, and 30 mol% during assembly. AFM characterization of dehydrated films revealed that both the apparent thickness and surface roughness *Rq* decreased with increasing cholesterol (Figure 3d and Figures S15 and S16). Interestingly, C18 lipid

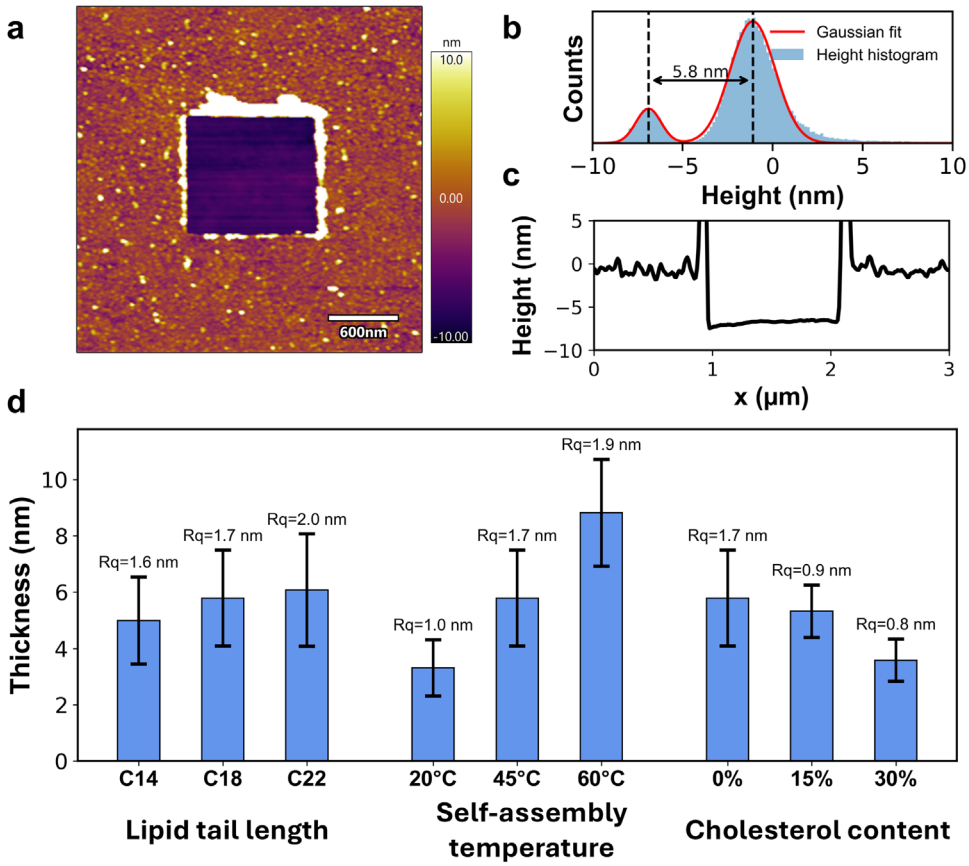

FIGURE 3 | Structural characterization of lipid assemblies. (a) AFM topography of the C18 lipid-assembled structure, with the central region scratched under a 100 nN applied force. (b) Height histogram determined from AFM. (c) Section profile across the scratched and intact regions, highlighting the step height of the assembled layer. (d) Summary of lipid layer thickness under various assembly conditions, with corresponding surface roughness values (*Rq*) shown as error bars. Lipid tail length experiments were conducted for samples assembled at 45°C (left), temperature-dependent studies were performed using C18 (middle), and cholesterol-content experiments were conducted with C18 lipid assembled at 45°C (right).

films formed with 30 mol% cholesterol were strikingly smooth with low surface roughness values $Rq \approx 0.75$ nm (Figure S17). Although cholesterol has been previously reported to increase bilayer thickness in hydrated vesicles, our measurements reveal an opposite trend for dehydrated lipid films. Incorporation of cholesterol enhances the ordering of acyl chains which reduces the amount of available residual free volume upon drying, yielding smoother and more compact films that undergo minimal structural changes during dehydration. In contrast, cholesterol-free C18 films exhibit increased heterogeneities with a larger surface roughness.

2.3 | Electronic Characterization

A liquid metal electrode technique (EGaIn) was used to characterize the electronic properties of polymer-supported lipid assemblies. The EGaIn method relies on using a liquid metal alloy as a soft electrical contact for capacitance (or conductivity) measurements. This approach enables characterization of self-assembled molecular monolayers or bilayers without significantly affecting their underlying structure [21]. In this way, a parallel-plate capacitor geometry was formed using gold as the bottom electrode and EGaIn liquid metal as the top electrode (Figure 1).

We began by determining the leakage current behavior and breakdown voltage of lipid layers, which are critical parameters for functional dielectric materials. Using the EGaIn setup, we first measured the current–voltage (I–V) response of C14, C18, and C22 lipid films prepared at 45°C with no cholesterol (Figure 4a). A weak current response was observed upon sweeping the voltage between −1 and 1 V, with current densities reaching approximately 10^{-5} A cm^{-2} at ± 1 V (Figure 4a). This current leakage is comparable to typical inorganic dielectrics such as ZrO_2 (3.2×10^{-5} A cm^{-2} at 2 V for a 12.5 nm film) [50], highlighting the superb electronic insulating qualities of self-assembled lipid layers. The relatively low leakage current density suggests that the lipid films are largely free of macroscopic pinholes that would result in direct liquid metal contact with the gold electrode. Comparing lipids of different tail lengths, C18 and C22 samples exhibited similar leakage currents, whereas the C14 film showed slightly higher leakage current values, which is attributed to the reduced thickness of the C14 layer. In these devices, the assembled lipid layer functions as a tunneling barrier, and the tunneling probability decreases exponentially with barrier thickness [51]. We further evaluated the breakdown voltage of each sample by linearly ramping the applied bias until electrical shorting (Figure 4b). Our results show that the thinnest lipid film (C14) exhibited breakdown at 4.2 V, followed by C18 at 4.8 V and C22 at 5.1 V. Overall, these results are consistent with the expectation

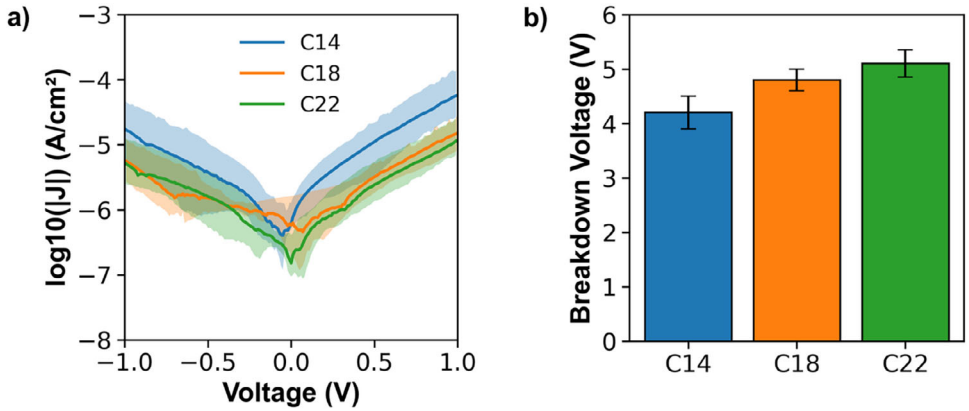

FIGURE 4 | Electronic properties of assembled lipid films. (a) Current–voltage (*I–V*) curves of lipid-assembled layers prepared at 45°C with no cholesterol, where the shaded regions represent the 25th–75th percentile range of measured currents. (b) Breakdown voltages of the same lipid-assembled layers, obtained by linearly sweeping the applied voltage from 0 to 6 V. Error bars represent the standard deviation from five independent measurements acquired at different locations on the same sample.

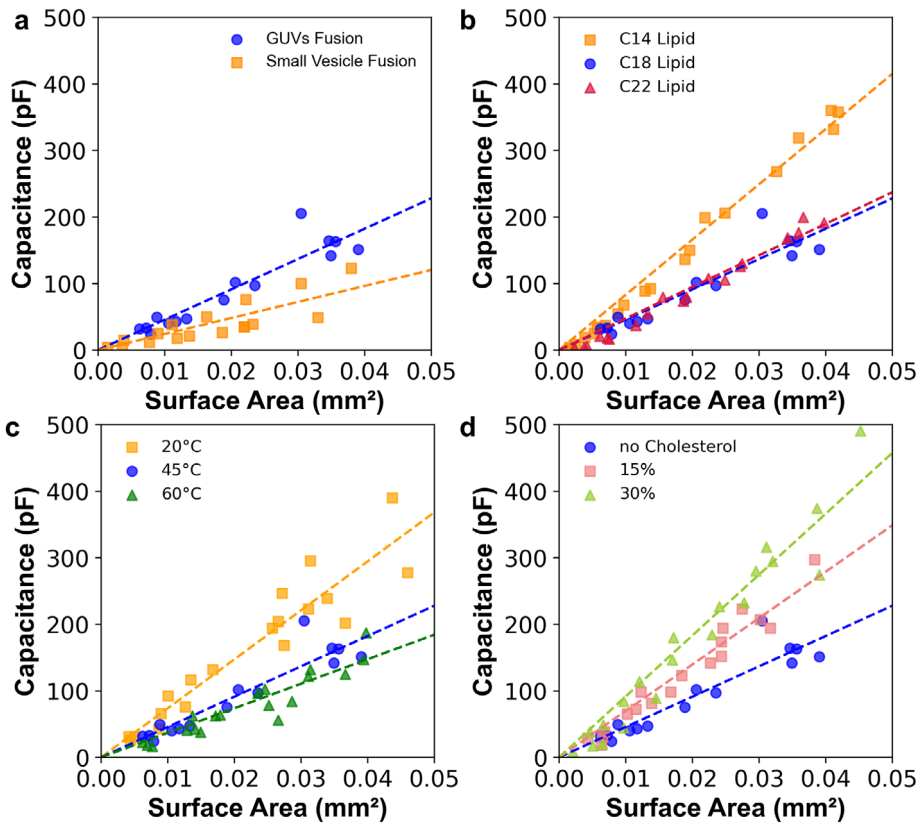

FIGURE 5 | Capacitance as a function of electrode surface area for lipid layers assembled under different conditions as a function of: (a) preparation method for C18 lipid layers assembled at 45°C, (b) lipid tail length for samples assembled at 45°C, (c) assembly temperature for lipid C18, and (d) varying cholesterol content for C18 lipid layers.

that thicker dielectric layers can sustain higher electric fields before electrical breakdown.

We further measured the capacitance of assembled lipid layers using an inductance-capacitance-resistance (LCR) meter (Figure 5). For these experiments, the contact area between the liquid metal electrode and the lipid interface was determined by imaging, and the corresponding capacitance values were measured at 0.5 V at 10 kHz and plotted as a function of the contact area (Figure S18). We first compared the capacitance measurements for C18 layers assembled by small lipid vesicle fusion and GUV fusion at 45°C (Figure 5a). Results from the measured capacitance vs. contact area were analyzed using linear regression, yielding a slope of 4.3 ± 0.3 nF/mm^2 for C18 GUV sam-

ple and 2.4 ± 0.2 nF/mm^2 for C18 small lipid vesicle sample. The measured capacitance values are comparable to those reported in foundational molecular-electronics studies of fatty acid salt monolayers [20]. Comparing the two assembly approaches, the larger capacitance per area of the GUV-fused layer is attributed to higher structural uniformity achieved using this method of preparation (Figure 2). We posit that the GUV-fused layers reduce the effective dielectric thickness and minimize defects by decreasing surface heterogeneity, thereby increasing the film capacitance. Overall, the GUV-fusion assembly method improves reproducibility in surface structural properties and electrical characterization experiments.

We next characterized the dielectric properties of the assembled lipid films. The dielectric constant (or relative permittivity) ε_r reflects the ability of a material to store charge in charge-separating media. Based on the structure of a lipid molecule, the hydrophilic head region is expected to exhibit a larger dipole moment compared to the hydrophobic tail region [52]. To determine the dielectric constant of self-assembled lipid layers, we used an expression for a parallel-plate capacitor:

$$C = \varepsilon_0 \varepsilon_r \frac{A}{d} \quad (1)$$

where C is the capacitance, ε_r is the dielectric constant of the material, $\varepsilon_0$is the vacuum permittivity, A is the electrode area, and d is the dielectric layer thickness. Using this approach, we determined the dielectric constant ε_r of the assembled lipid layers using experimentally measured values of the capacitance C, contact area A, and film thickness d. We systematically studied a series of conditions for lipid assembly by varying lipid tail length, assembly temperature, and cholesterol content, which are known to strongly influence lipid membrane structures [47, 53–55].

We first examined the effect of lipid tail length on capacitance using an assembly temperature of 45°C in the absence of cholesterol. As shown in Figure 5b, the C14 lipid layers exhibit a larger specific capacitance, whereas the C18 and C22 samples showed similar capacitance values. This observation is consistent with the current–voltage (I–V) behavior, where C18 and C22 exhibited similar I–V responses, but C14 showed slightly larger leakage currents. The larger capacitance observed for C14 was attributed to its smaller film thickness, consistent with the inverse relationship between capacitance and layer thickness based on the parallel-plate capacitor relation (Equation 1). C14 exhibits a larger influence of its polar head group relative to the nonpolar tail, which likely contributes to a higher dielectric response. Overall, these results indicate that lipid tail length plays a key role in determining the dielectric properties of the assembled layers.

We next characterized the capacitance of C18 lipid layers assembled at different temperatures (Figure 5c). Lipid layers formed at 20°C exhibited the highest specific capacitance (7.3 ± 0.3 nF mm^{-2}), whereas lipids assembled at 60°C showed the smallest capacitance value (3.8 ± 0.2 nF mm^{-2}), which is consistent with the inverse relationship between capacitance and dielectric layer thickness. We further calculated the dielectric constants based on Equation 1, obtaining values of 2.8 ± 0.1 for both 20°C and 45°C samples, and increasing to 3.8 ± 0.2 at 60°C. These results suggest that although the dielectric response remains similar at lower assembly temperatures, lipid assemblies formed at elevated temperatures become less ordered. We hypothesize that disordered lipid layers provide additional space for dipolar reorientation of the polar headgroups, leading to enhanced polarization and a larger effective dielectric constant [56–58]. In contrast, more tightly packed layers formed at lower temperature restrict dipole mobility, resulting in a lower dielectric response.

We further analyzed the capacitance of the C18 layers with varying cholesterol content (Figure 5d). The thinnest lipid layer with 30% cholesterol exhibited the highest specific capacitance (9.1 ± 0.3 nF mm^{-2}), followed by 15% cholesterol (7.0 ± 0.2 nF mm^{-2}), and the 0% cholesterol lipid sample (4.3 ± 0.2 nF mm^{-2}). The corresponding dielectric constants were 3.7 ± 0.1 for 30% cholesterol, 4.2 ± 0.1 for 15% cholesterol, and 2.8 ± 0.1 for the pristine film, indicating that cholesterol incorporation generally enhances the dielectric response. We attribute the overall increase in dielectric constant for samples containing cholesterol to a higher molecular packing density, which increases the number of dipolar units per unit area [59]. The slight decrease in dielectric constant upon increasing cholesterol content from 15% to 30% is attributed to an increase in packing density, such that lipid films become highly ordered, restricting dipolar reorientation of the lipid headgroups along with the addition of the nonpolar cholesterol molecule, which effectively dilutes the fraction of polar headgroups at high cholesterol content.

3 | Conclusions

In this work, we show that self-assembled lipids serve as effective soft dielectric materials. Using a vesicle fusion method on polymer-coated gold electrodes, we demonstrate uniform and continuous lipid films suitable for direct electrical characterization using a liquid-metal electrode technique (EGaIn). Systematic variation of lipid tail length, assembly temperature, and cholesterol content shows clear trends in structure-property relationships. Interestingly, the film thickness trends observed under different assembly conditions are generally opposite to those reported for hydrated lipid bilayers, indicating that lipid structural ordering during dehydration is influenced by processing conditions during assembly and fabrication. In addition, temperature and cholesterol-dependent electronic characterization experiments show that when the hydrated, solid-supported lipid layers are assembled in a densely packed state, dehydration induces minimal structural reorganization. In this way, the dehydrated lipid films exhibit low surface roughness values similar to the original bilayer structure. Overall, this work establishes new avenues for using self-assembled lipid-based materials as a promising strategy for fabricating ultrathin dielectric films for soft bioelectronic applications.

4 | Materials and Methods

4.1 | Lipid Handling and Electroformation of GUVs

All lipids were purchased from Avanti Polar Lipids, Inc. (Alabaster, AL, USA) and used as received. Giant unilamellar

vesicles (GUVs) of varying compositions were prepared using the electroformation method as previously described [60]. Lipid mixtures containing the specified phospholipids and cholesterol were dissolved in chloroform and deposited onto indium tin oxide (ITO)-coated glass slides (25 mm × 75 mm, NanoCS, Inc.) by spin-coating. The lipid-coated slides were subsequently desiccated under vacuum for at least 3 h to ensure removal of residual solvent. Polydimethylsiloxane (PDMS) spacers (5 mm thickness) were fabricated using SYLGARD 184 Silicone Elastomer Kit (Dow Chemical Company) with a 10:1 base-to-curing agent ratio. The mixture was degassed under vacuum, poured into molds, and cured at 60°C for 3 h. After curing, the PDMS slabs were cut to match the dimensions of the glass slides.

Electroformation chambers were assembled by sandwiching two ITO-coated slides face-to-face with the PDMS spacer positioned between them. The chamber was filled with pure water and secured with clamps. Electroformation was performed by applying a sinusoidal electric field at 1 V/mm and 10 Hz for 4.5 h at 45 degrees using a function generator. GUVs formed with the electroformation process were imaged using fluorescence microscopy (Figures S3 and S4) for samples containing lissamine rhodamine B sulfonyl (Rhod-PE 18:1, Avanti Polar Lipids, Inc.) as a fluorescent lipid marker (typically 0.5–1 mol%), and phase contrast microscopy for unlabeled samples.

For the vesicle fusion process, surface-modified gold substrates were copiously rinsed with deionized water and dried under vacuum. The dried substrates were then placed in small glass vials, and the GUV suspension was slowly injected into each vial. The vials were sealed and incubated at 20°C, 45°C, or 60°C for 3 h to promote vesicle rupture and fusion onto the gold surface. Following incubation, the gold substrates were carefully removed from the vials and gently rinsed with deionized water using indirect flow to avoid direct spray onto the surface. The rinsed substrates were then desiccated under vacuum prior to subsequent measurements. For direct visualization of vesicle rupture and supported bilayer formation, surface-treated glass coverslips were used in place of gold substrates. The adsorption process was monitored in real-time using fluorescence microscopy, which allowed observation of vesicle adhesion, rupture, and fusion on the surface.

4.2 | Contact Angle Measurements

Contact angle measurements were performed to determine the surface wetting properties under different conditions. Static water contact angles were measured using a Ramé-Hart Model 250 contact angle goniometer via the sessile drop method. For each sample, ten measurements were performed over different regions and averaged to determine statistical mean values.

4.3 | ATR-FTIR

Attenuated total reflectance-Fourier transform infrared (ATR-FTIR) spectroscopy was performed using a Thermo Nicolet iS50 FTIR to evaluate the chemical composition of the assembled layer. For pure lipid samples, a solution containing lipid molecules was first deposited onto the ATR crystal, and the solvent was allowed to fully evaporate. ATR-FTIR analysis was then performed on the dried lipid molecules on the surface. For measurements involving gold substrates, the substrate surfaces were pressed directly onto the ATR crystal for data collection.

4.4 | Atomic Force Microscopy

Atomic force microscopy (AFM) was employed to characterize both the surface morphology and assembled layer thickness. Surface topography measurements were performed in tapping mode using an Asylum Research MFP-3D AFM equipped with Tap300Al-G probes. To determine the layer thickness, a 1 μm^2 central region was scratched using the AFM tip. Prior to scratching, the cantilever spring constant was calibrated to ensure accurate force control. As a control experiment, a normal force of 200 nN was applied to a bare Au substrate, confirming that this load did not induce damage to the gold surface (Figure S5). Subsequently, the films were locally removed under contact mode by applying a constant force of 100 nN. The resulting height step between the scratched and unscratched regions was visualized by extracting line profiles across the boundary. For quantitative thickness determination, height histograms were generated from topography data and analyzed by fitting two Gaussian distributions, corresponding to the exposed Au surface and the intact lipid layers. The thickness was determined from the separation between the two Gaussian peak positions.

4.5 | Preparation of Gold Electrode Surfaces

We used template-stripped gold (Au^{TS}) substrates for self-assembly owing to the exceptional flatness of these surfaces (RMS roughness ≈0.4 nm over a 5 μm × 5 μm area scan). Au^{TS} substrates were fabricated from clean silicon wafers. The Si wafers were first subjected to a standard cleaning procedure involving sequential sonication in isopropyl alcohol, acetone, and isopropyl alcohol again, each for 15 min. Subsequently, a 200 nm gold layer was deposited onto the Si wafer using electron-beam evaporation at a rate of 0.5 Å s^{-1}. A droplet of Norland 61 optical adhesive was then deposited onto the gold surface, followed by pressing a cleaned glass strip onto the adhesive. After UV curing, the gold layer was firmly bonded to the glass support. Immediately prior to lipid deposition and self-assembly, the glass strip was gently striped away from the Si wafer. Because of the inherently weak adhesion between gold and silicon, this process exposes the gold surface that was in contact with the Si template. The resulting exposed surface is atomically smooth and provides an ideal platform for high-quality self-assembled layers.

Prior to lipid assembly, we first formed a poly-D-lysine (PDL) self-assembled monolayer on Au^{TS} substrates by immersing the freshly prepared Au^{TS} in a PDL solution (0.1 mg mL^{-1} in PBS). The thin PDL coating significantly reduced the surface hydrophobicity of gold. After incubation at room temperature for 1 h, the sample was removed and thoroughly rinsed with deionized (DI) water to eliminate excess PDL molecules. The resulting PDL layer was determined to be ~0.9 nm in thickness.

The film was then dried under a gentle stream of nitrogen and further dried under vacuum.

For vesicle fusion, PDL-functionalized gold surfaces were immersed in a vesicle suspension prepared via electroformation. The incubation was carried out at the target temperature for 3 h to ensure complete surface coverage through vesicle fusion. After incubation, the sample was gently rinsed with excess DI water to remove any multilamellar aggregates, followed by drying under a nitrogen stream and subsequent vacuum drying for at least 12 h.

4.6 | EGaIn//Self Assembled Layer//AuTS Measurement

Electronic measurements were performed using a two-electrode configuration as previously described [35]. Au^{TS} served as the bottom electrode, whereas conical tips of eutectic gallium-indium (EGaIn) alloy liquid metal were used as the top contact. The experimental setup was constructed on a vibrationally isolated optical table (Newport) to minimize mechanical instabilities. Liquid metal manipulation and contact establishment were executed using a Zaber motorized translation stage, which offers a resolution down to 0.03 μm/s.

Capacitance measurements were performed using a BK Precision 891 LCR meter in a four-wire configuration, with a 0.5 V AC excitation at 10 kHz. The measurements were conducted in the parallel (Cp–Rp) mode, which is most suitable for high-resistance dielectric films. Lipid assembled layers exhibit low leakage currents and behave as nearly ideal capacitors with a small parallel leakage resistance; thus, the Cp model provides an accurate description of the electrical response. For each sample, approximately 20 independent contact points were probed, and the capacitance (Cp) was recorded. A digital camera was used concurrently to image each contact event, and the captured images were analyzed to determine the effective contact cross-sectional area. These values were subsequently used for quantitative capacitance–area analysis.

To determine an appropriate measurement frequency, we performed frequency-dependent scans of Cp as shown in Figure S3. The capacitance exhibited a slight decrease with increasing frequency, consistent with the expected dielectric dispersion of molecular films: at low frequencies, slow polarization processes such as dipolar reorientation and interfacial charge accumulation contribute to a higher apparent permittivity, whereas at higher frequencies, only the faster electronic and atomic polarizations can respond, resulting in a lower effective capacitance. A frequency of 10 kHz was chosen to ensure stable measurements while retaining sensitivity to organic molecule dipolar and interfacial polarization processes that diminish at higher frequencies.

Breakdown voltage measurements were carried out using a Keithley 1602B source-measure unit (SMU). After establishing electrical contact, the voltage was linearly swept from 0 to 6 V with a step size of 0.01 V and a dwell time of 0.005 s per step. The breakdown voltage was identified as the point at which a sudden increase in current was observed, indicating dielectric failure of the film.

Acknowledgements

This research was supported by U.S. Department of Energy, Office of Science, Basic Energy Sciences under Award number DE-SC0022035 and the National Science Foundation Award 2227399.

Conflicts of Interest

The authors declare no conflicts of interest.

Data Availability Statement

The data that support the findings of this study are available from the corresponding author upon reasonable request.

References

1. K. Kobayashi, K. Endo, and H. Wada, *Lipids in Plant and Algae Development*, Edited by Y. Nakamura and Y. Li-Beisson (Springer International Publishing, 2016), 21–49, https://doi.org/10.1007/978-3-319-25979-6.

2. R. N. McElhaney, "Membrane Lipid Not Polarized Water Is Responsible for the Semipermeable Properties of Living Cells," *Biophysical Journal* 15 (1975): 777–784, https://doi.org/10.1016/S0006-3495(75)85854-1.

3. S. Abraham, T. Heckenthaler, Y. Morgenstern, and Y. Kaufman, "Effect of Temperature on the Structure Electrical Resistivity and Charge Capacitance of Supported Lipid Bilayers," *Langmuir* 35 (2019): 8709–8715, https://doi.org/10.1021/acs.langmuir.9b00726.

4. D. W. Kim, S.-W. Kim, and U. Jeong, "Lipids: Source of Static Electricity of Regenerative Natural Substances and Nondestructive Energy Harvesting," *Advanced Materials* 30 (2018): 1804949, https://doi.org/10.1002/adma.201804949.

5. B. P. Bean, "The Action Potential in Mammalian Central Neurons," *Nature Reviews Neuroscience* 8 (2007): 451–465, https://doi.org/10.1038/nrn2148.

6. P. Mueller and D. O. Rudin, "Action Potential Phenomena in Experimental Bimolecular Lipid Membranes," *Nature* 213 (1967): 603–604, https://doi.org/10.1038/213603a0.

7. J. T. Kindt, J. W. Szostak, and A. Wang, "Bulk Selfassembly of Giant Unilamellar Vesicles," *ACS Nano* 14 (2020): 14627–14634, https://doi.org/10.1021/acsnano.0c03125.

8. C. Dumas, R. El Zein, H. Dallaporta, and A. M. Charrier, "Autonomic Selfhealing Lipid Monolayer a New Class of Ultrathin Dielectric Lipid Monolayer: A New Class of Ultrathin Dielectric," *Langmuir* 27 (2011): 13643–13647, https://doi.org/10.1021/la202333n.

9. S. E. Kim, J. Y. Sung, J. D. Jeon, et al., "Toward Advanced High-k and Electrode Thin Films for DRAM Capacitors via Atomic Layer Deposition," *Advanced Materials Technologies* 8 (2023): 2200878, https://doi.org/10.1002/admt.202200878.

10. K. S. Tang, W. S. Lau, and G. S. Samudra, "Trends in DRAM Dielectrics," *IEEE Circuits and Devices Magazine* 13 (1997): 27–34, https://doi.org/10.1109/101.589261.

11. S. E. Kim, J. Y. Sung, Y. Yun, et al., "Atomic Layer Deposition of High-k and Metal Thin Films for High-Performance DRAM Capacitors: A Brief Review," *Current Applied Physics* 64 (2024): 8–15, https://doi.org/10.1016/j.cap.2024.05.011.

12. Y. Lee, J. W. DuMont, and S. M. George, "Trimethylaluminum as the Metal Precursor for the Atomic Layer Etching of Al_2O_3 Using Sequential, Self-Limiting Thermal Reactions," *Chemistry of Materials* 28 (2016): 2994–3003, https://doi.org/10.1021/acs.chemmater.6b00111.

13. S. M. George and Y. Lee, "Prospects for Thermal Atomic Layer Etching Using Sequential, Self-Limiting Fluorination and Ligand-Exchange Reactions," *ACS Nano* 10 (2016): 4889–4894, https://doi.org/10.1021/acsnano.6b02991.

14. R. Naumann, S. M. Schiller, F. Giess, et al., "Tethered Lipid Bilayers on Ultraflat Gold Surfaces," *Langmuir* 19 (2003): 5435–5443, https://doi.org/10.1021/la0342060.

15. M. D. Muzio, R. Millan-Solsona, J. H. Borrell, L. Fumagalli, and G. Gomila, "Cholesterol Effect on the Specific Capacitance of Submicrometric DOPC Bilayer Patches Measured by in-Liquid Scanning Dielectric Microscopy," *Langmuir* 36 (2020): 12963–12972, https://doi.org/10.1021/acs.langmuir.0c02251.

16. A. Kenaan, R. El Zein, V. Kilinc, S. Lamant, J.-M. Raimundo, and A. M. Charrier, "Ultrathin Supported Lipid Monolayer With Unprecedented Mechanical and Dielectric Properties," *Advanced Functional Materials* 28 (2018): 1801024, https://doi.org/10.1002/adfm.201801024.

17. A. Gennaro, O. Deschaume, H. Pfeiffer, C. Bartic, P. Wagner, and M. Wübbenhorst, "Understanding the Dehydration Stress in Lipid Vesicles by a Combined Quartz Crystal Microbalance and Dielectric Spectroscopy Study," *Physica Status Solidi (a)* 217 (2020): 1900986.

18. J. Kurniawan, J. F. Ventrici de Souza, A. T. Dang, G. Liu, and T. L. Kuhl, "Preparation and Characterization of Solid-Supported Lipid Bilayers Formed by Langmuir–Blodgett Deposition: A Tutorial," *Langmuir* 34 (2018): 15622–15639, https://doi.org/10.1021/acs.langmuir.8b03504.

19. X. D. Cui, X. Zarate, J. Tomfohr, et al., "Making Electrical Contacts to Molecular Monolayers," *Nanotechnology* 13 (2001): 5–14, https://doi.org/10.1088/0957-4484/13/1/302.

20. B. Mann and H. Kuhn, "Tunneling Through Fatty Acid Salt Monolayers," *Journal of Applied Physics* 42 (1971): 4398–4405, https://doi.org/10.1063/1.1659785.

21. R. C. Chiechi, E. A. Weiss, M. D. Dickey, and G. M. Whitesides, "Eutectic Gallium–Indium (EGaIn): A Moldable Liquid Metal for Electrical Characterization of Self-Assembled Monolayers," *Angewandte Chemie International Edition* 47 (2008): 142–144, https://doi.org/10.1002/anie.200703642.

22. Z. Bian, E. Gomez, J. Ren, et al., "Ultrathin Atomically Flat Gold Film for Scanning Tunneling Microscopy and Single-Particle Fluorescence Spectroscopy," *Langmuir* 41 (2025): 16000–16008, https://doi.org/10.1021/acs.langmuir.5c01097.

23. P. S. Cremer and S. G. Boxer, "Formation and Spreading of Lipid Bilayers on Planar Glass Supports," *The Journal of Physical Chemistry B* 103 (1999): 2554–2559, https://doi.org/10.1021/jp983996x.

24. S. V. Bennun, R. Faller, and M. L. Longo, "Drying and Rehydration of DLPC/DSPC Symmetric and Asymmetric Supported Lipid Bilayers: A Combined AFM and Fluorescence Microscopy Study," *Langmuir* 24 (2008): 10371–10381, https://doi.org/10.1021/la8016694.

25. E. P. Ivanova, D. K. Pham, N. Brack, P. Pigram, and D. V. Nicolau, "Poly(l-lysine)-Mediated Immobilisation of Oligonucleotides on Carboxy-Rich Polymer Surfaces," *Biosensors and Bioelectronics* 19 (2004): 1363–1370, https://doi.org/10.1016/j.bios.2003.12.030.

26. Y. Kaufman, A. Berman, and V. Freger, "Supported Lipid Bilayer Membranes for Water Purification by Reverse Osmosis," *Langmuir* 26 (2010): 7388–7395, https://doi.org/10.1021/la904411b.

27. C. A. Keller, K. Glasmästar, V. P. Zhdanov, and B. Kasemo, "Formation of Supported Membranes From Vesicles," *Physical Review Letters* 84 (2000): 5443–5446, https://doi.org/10.1103/PhysRevLett.84.5443.

28. C. F. de Freitas, I. R. Calori, A. L. Tessaro, W. Caetano, and N. Hioka, "Rapid Formation of Small Unilamellar Vesicles (SUV) Through Low-Frequency Sonication: An Innovative Approach," *Colloids and Surfaces B: Biointerfaces* 181 (2019): 837–844.

29. Z. Boban, I. Mardešić, W. K. Subczynski, and M. Raguz, "Giant Unilamellar Vesicle Electroformation: What to Use, What to Avoid, and How to Quantify the Results," *Membranes* 11 (2021): 860, https://doi.org/10.3390/membranes11110860.

30. C. A. Keller, K. Glasmästar, V. P. Zhdanov, and B. Kasemo, "Formation of Supported Membranes from Vesicles," *Physical Review Letters* 84, no. 23 (2000): 5443–5446, https://doi.org/10.1103/physrevlett.84.5443.

31. E. Reimhult, F. Höök, and B. Kasemo, "Intact Vesicle Adsorption and Supported Biomembrane Formation from Vesicles in Solution: Influence of Surface Chemistry, Vesicle Size, Temperature, and Osmotic Pressure," *Langmuir* 19, no. 5 (2002): 1681–1691, https://doi.org/10.1021/la0263920.

32. E. Reimhult, F. Höök, and B. Kasemo, "Vesicle Adsorption on SiO_2 and TiO_2: Dependence on Vesicle Size," *The Journal of Chemical Physics* 117, no. 16 (2002): 7401–7404, https://doi.org/10.1063/1.1515320.

33. R. P. Richter, R. Bérat, and A. R. Brisson, "Formation of Solid-Supported Lipid Bilayers: An Integrated View," *Langmuir* 22, no. 8 (2006): 3497–3505, https://doi.org/10.1021/la052687c.

34. C. Hamai, P. S. Cremer, and S. M. Musser, "Single Giant Vesicle Rupture Events Reveal Multiple Mechanisms of Glass-Supported Bilayer Formation," *Biophysical Journal* 92, no. 6 (2007): 1988–1999, https://doi.org/10.1529/biophysj.106.093831.

35. H. Yang, X. Liu, M. Meigooni, et al., "Amino Acid Sequence Controls Enhanced Electron Transport in Heme-Binding Peptide Monolayers," *ACS Central Science* 11 (2025): 612–621, https://doi.org/10.1021/acscentsci.4c01849.

36. N. Kučerka, J. F. Nagle, J. N. Sachs, et al., "Lipid Bilayer Structure Determined by the Simultaneous Analysis of Neutron and X-Ray Scattering Data," *Biophysical Journal* 95 (2008): 2356–2367.

37. S. Tristram-Nagle, H. I. Petrache, and J. F. Nagle, "Structure and Interactions of Fully Hydrated Dioleoylphosphatidylcholine Bilayers," *Biophysical Journal* 75 (1998): 917–925, https://doi.org/10.1016/S0006-3495(98)77580-0.

38. M. C. Wiener, G. I. King, and S. H. White, "Structure of a Fluid Dioleoylphosphatidylcholine Bilayer Determined by Joint Refinement of X-Ray and Neutron Diffraction Data. I. Scaling of Neutron Data and the Distributions of Double Bonds and Water," *Biophysical Journal* 60 (1991): 568–576, https://doi.org/10.1016/S0006-3495(91)82086-0.

39. M. C. Wiener and S. H. White, "Structure of a Fluid Dioleoylphosphatidylcholine Bilayer Determined by Joint Refinement of X-Ray and Neutron Diffraction Data. II. Distribution and Packing of Terminal Methyl Groups," *Biophysical Journal* 61 (1992): 428–433, https://doi.org/10.1016/S0006-3495(92)81848-9.

40. M. C. Wiener and S. H. White, "Structure of a Fluid Dioleoylphosphatidylcholine Bilayer Determined by Joint Refinement of X-Ray and Neutron Diffraction Data. III. Complete Structure," *Biophysical Journal* 61 (1992): 434–447, https://doi.org/10.1016/S0006-3495(92)81849-0.

41. S. S. Stachura, C. J. Malajczuk, E. Kuprusevicius, and R. L. Mancera, "Influence of Bilayer Size and Number in Multi-Bilayer DOPC Simulations at Full and Low Hydration," *Langmuir* 35 (2019): 2399–2411, https://doi.org/10.1021/acs.langmuir.8b03212.

42. K. L. Koster, M. S. Webb, G. Bryant, and D. V. Lynch, "Interactions Between Soluble Sugars and POPC (1-Palmitoyl-2-Oleoylphosphatidylcholine) During Dehydration: Vitrification of Sugars Alters the Phase Behavior of the Phospholipid," *Biochimica et Biophysica Acta (BBA)—Biomembranes* 1193 (1994): 143–150, https://doi.org/10.1016/0005-2736(94)90343-3.

43. P. L. G. Chong and A. R. Cossins, "Interacting Effects of Temperature, Pressure and Cholesterol Content Upon the Molecular Order of Dioleoylphosphatidylcholine Vesicles," *Biochimica et Biophysica Acta (BBA)—Biomembranes* 772 (1984): 197–201, https://doi.org/10.1016/0005-2736(84)90044-0.

44. J. Pan, S. Tristram-Nagle, N. Kučerka, and J. F. Nagle, "Temperature Dependence of Structure, Bending Rigidity, and Bilayer Interactions of Dioleoylphosphatidylcholine Bilayers," *Biophysical Journal* 94 (2008): 117–124, https://doi.org/10.1529/biophysj.107.115691.

45. N. Kučerka, M.-P. Nieh, and J. Katsaras, "Fluid Phase Lipid Areas and Bilayer Thicknesses of Commonly Used Phosphatidylcholines as a Function of Temperature," *Biochimica et Biophysica Acta (BBA)—Biomembranes* 2011 (1808): 2761–2771.

46. Z. V. Leonenko, E. Finot, H. Ma, T. E. S. Dahms, and D. T. Cramb, "Investigation of Temperature-Induced Phase Transitions in DOPC and

DPPC Phospholipid Bilayers Using Temperature-Controlled Scanning Force Microscopy," *Biophysical Journal* 86 (2004): 3783–3793, https://doi.org/10.1529/biophysj.103.036681.

47. F. T. Doole, T. Kumarage, R. Ashkar, and M. F. Brown, "Cholesterol Stiffening of Lipid Membranes," *The Journal of Membrane Biology* 255 (2022): 385–405, https://link.springer.com/article/10.1007/s00232-022-00263-9.

48. X. Xu and E. London, "The Effect of Sterol Structure on Membrane Lipid Domains Reveals How Cholesterol Can Induce Lipid Domain Formation," *Biochemistry* 39 (2000): 843–849, https://doi.org/10.1021/bi992543v.

49. M. Alwarawrah, J. Dai, and J. Huang, "A Molecular View of the Cholesterol Condensing Effect in DOPC Lipid Bilayers," *The Journal of Physical Chemistry B* 114 (2010): 7516–7523, https://doi.org/10.1021/jp101415g.

50. D. Q. Xiao, G. He, J. G. Lv, et al., "Interfacial Modulation and Electrical Properties Improvement of Solution-Processed ZrO_2 Gate Dielectrics Upon Gd Incorporation," *Journal of Alloys and Compounds* 699 (2017): 415–420.

51. L. Cademartiri, M. M. Thuo, C. A. Nijhuis, et al., "Electrical Resistance of Ag^{TS} $-S(CH_2)_{n-1}$ $CH_3//Ga_2O_3$ /EGaIn Tunneling Junctions," *The Journal of Physical Chemistry C* 116 (2012): 10848–10860, https://doi.org/10.1021/jp212501s.

52. Y. A. Ermakov, "Electric Fields at the Lipid Membrane Interface," *Membranes* 13 (2023): 883, https://doi.org/10.3390/membranes13110883.

53. S. L. Veatch and S. L. Keller, "Seeing Spots: Complex Phase Behavior in Simple Membranes," *Biochimica et Biophysica Acta (BBA)—Molecular Cell Research* 1746 (2005): 172–185, https://doi.org/10.1016/j.bbamcr.2005.06.010.

54. J. F. Nagle and S. Tristram-Nagle, "Structure of Lipid Bilayers," *Biochimica et Biophysica Acta (BBA)—Reviews on Biomembranes* 1469 (2000): 159–195, https://doi.org/10.1016/S0304-4157(00)00016-2.

55. H. Ohvo-Rekilä, B. Ramstedt, P. Leppimäki, and J. Peter Slotte, "Cholesterol Interactions With Phospholipids in Membranes," *Progress in Lipid Research* 41 (2002): 66–97, https://doi.org/10.1016/S0163-7827(01)00020-0.

56. Z. Pan, L. Li, F. Jin, et al., "Dipole Orientation Engineering in Crosslinking Polymer Blends for High-Temperature Energy Storage Applications," *Advanced Science* 11 (2024): 2405730, https://doi.org/10.1002/advs.202405730.

57. Y. Hidaka and K. Asami, "Measurement of Dipole Potential in Bilayer Lipid Membranes by Dielectric Spectroscopy," *The Journal of Membrane Biology* 247 (2014): 721–727, https://doi.org/10.1007/s00232-014-9697-1.

58. L. Yang, X. Liu, Z. Lu, et al., "Free volume Dependence of the Dielectric Constant of Poly (Vinylidene Fluoride) Nanocomposite Films," *RSC Advances* 12 (2022): 24734–24772.

59. S. Chakraborty, M. Doktorova, T. R. Molugu, et al., "How Cholesterol Stiffens Unsaturated Lipid Membranes," *Proceedings of the National Academy of Sciences* 117 (2020): 21896–21905, https://doi.org/10.1073/pnas.2004807117.

60. D. Kumar, C. M. Richter, and C. M. Schroeder, "Conformational Dynamics and Phase Behavior of Lipid Vesicles in a Precisely Controlled Extensional Flow," *Soft Matter* 16 (2020): 337–347, https://doi.org/10.1039/C9SM02048A.

Supporting Information

Additional supporting information can be found online in the Supporting Information section.

Supporting File: adfm77643-sup-0001-SuppMat.pdf.